EXTENDING THE AREA SILENCED BY ACTIVE NOISE CONTROL USING MULTIPLE LOUDSPEAKERS

Annea Barkefors, Simon Berthilsson and Mikael Sternad

Signals and Systems, Uppsala University
Box 534, 751 21 Uppsala, Sweden, {anba,sibe,ms}@signal.uu.se

ABSTRACT

Active noise control is of increasing interest in e.g. cars, but the zone of noise damping becomes limited in reverberant environments. We investigate the possibility of extending this spatial zone significantly, by using multiple control loudspeakers. MIMO feedforward controllers designed by linear quadratic control theory are here shown to increase the limiting frequency for uniform damping in a 0.3×0.3 m test area, from 200 Hz to around 600 Hz.

1. INTRODUCTION

Noise is becoming an increasing problem in cars, partly because the push to lower fuel consumption by reducing weight tends to reduce the use of passive damping. Active noise control can reduce low-frequency noise by feedforward or feedback control [1]. Active systems in vehicles have been limited to the very lowest frequencies, see e.g. [2]. To the best of our knowledge, significant attenuation over useful spatial volumes has not been reported for frequencies above 200 Hz in car interiors.

When using a single loudspeaker, the zone of control is severely limited to a small fraction of the wavelength [3]. We here investigate the use of multiple loudspeakers to increase the upper limiting frequency for which uniform damping is attained within a target area. While other applications are conceivable, our investigation, performed in a room as outlined in Fig. 1, is primarily designed to guide ongoing investigations in vehicles. The use of continuous online adaptation and the use of a large number of active microphones in cars is problematic and expensive. Therefore we also explore the feasibility and accuracy requirements of designs based on pre-estimated models of acoustic transfer functions.

The use of multiple loudspeakers to control sound fields has received significant interest over the past decade. Three classes of methods have been proposed: Wave field synthesis,see e.g. [4], High Order Ambisonics [5] and multipoint Mean Square Error (MSE) designs, see e.g. [6] and [7]. Of these alternatives, only multipoint MSE design offers control over the time domain properties while not demanding unrealistic assumptions.

We here utilize an MSE feedforward control strategy based on LQG (Linear Quadratic Gaussian), or H_2, optimal control, using a polynomial equations approach to the design of filters and regulators. Compared to state-space methods, such solutions offer increased structural insight and also have good numerical properties. Compared to time domain matrix-based multipoint MSE optimization of FIR filters [8], we avoid the inversion of extremely large block-Toepliz matrices. Such methods, as well as adaptive tuning, would be impractical in the problem to be considered here, with many loudspeakers, control points and high order models and filters.

This research has been supported by the Swedish Research Council under contract 90552701 and by Dirac Research AB.

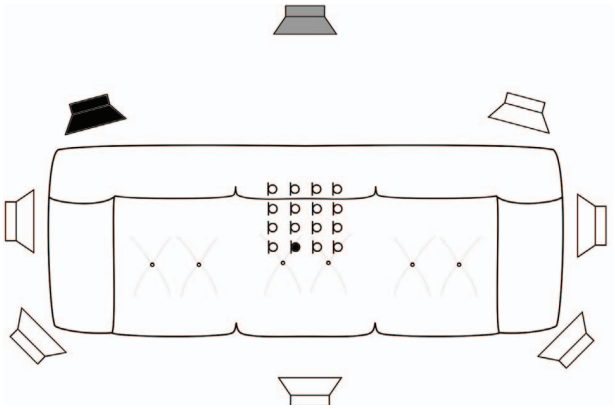

Fig. 1: The experimental setup, consisting of the noise speaker (gray) and seven control speakers (black and white), placed around a sofa with the 16 microphone positions, marked by '○' placed at ear height of a person sitting in it. The black loudspeaker and microphone are used in a SISO design for comparison.

The solution used here has been derived in [9]. A linear compensator in matrix fraction form is designed under stability and causality constraints. Frequency-dependent penalty weights can be used on the control errors and on the control signals in the quadratic design criterion. This feedforward regulator design has recently been applied successfully to problems of audio equalization and control of room acoustics, see [10] and [11].

The obtained results are promising. In particular, noise reduction above 10 dB is obtained over a 0.3×0.3 m area for frequencies up to 500 Hz with a causal feedforward filter, designed to suppress broadband noise. The design can be based on models of room transfer functions in FIR form, with realistically obtainable accuracy.

Notation: The transpose of a matrix $\mathbf{M}$ is denoted $\mathbf{M}'$. Matrices of causal FIR filters are represented by matrices $\boldsymbol{P}(q^{-1})$ of polynomials in the backward shift operator q^{-1}, where $v(t-1) = q^{-1}v(t)$ while $v(t+1) = qv(t)$ for discrete-time signal vectors $v(t)$. The time-domain operator q^{-1} corresponds to z^{-1} or $e^{-j\omega}$ in the frequency domain. For a polynomial matrix $\boldsymbol{P}(q^{-1})$, the corresponding conjugate matrix $\boldsymbol{P}_*(q)$ is defined as its conjugate transpose, with the forward shift operator q substituted for q^{-1} as arguments. Arguments are below omitted where there is no risk of misunderstanding.

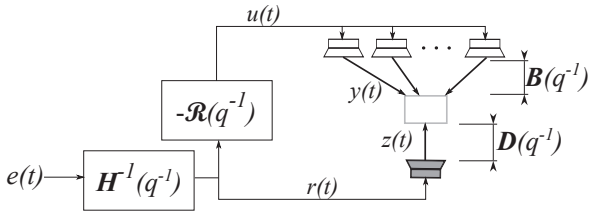

Fig. 2: A linear acoustic system is affected by L disturbances $r(t)$ through the primary paths $\boldsymbol{D}(q^{-1})$ to the volume of interest. N loudspeakers, with secondary paths $\boldsymbol{B}(q^{-1})$, are used by the feedforward regulator $\boldsymbol{\mathcal{R}}(q^{-1})$ to control the sound field within the volume of interest.

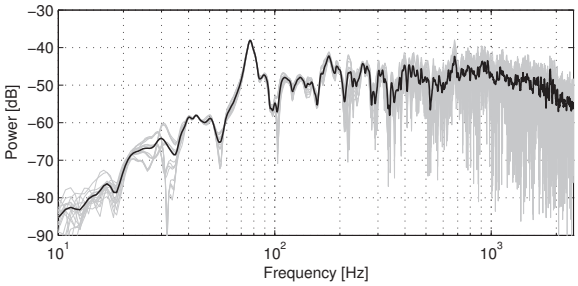

Fig. 3: The power spectral density from the noise speaker to all the microphone positions (gray), and their RMS average (black).

2. FEEDFORWARD ACTIVE NOISE CONTROL

A linear acoustic system is affected by L measurable disturbances, represented by a column vector $r(t)$, that are to be used for feedforward control, as illustrated in Fig. 2. The influence of these noise components is to be suppressed at M control points (measurement positions), by using a set of N loudspeakers where, in general, $N < M$. The control points are assumed located in the volume to be silenced, spaced by distances less than the spatial Nyquist frequency of the highest frequency sound to be controlled. The channels from the N control loudspeakers to the M positions (variously denoted forward paths, secondary paths or control paths) are represented by the FIR matrix model

$$y(t) = \boldsymbol{B}(q^{-1})\, u(t) \ . \tag{1}$$

Here, the $N \times 1$ vector $u(t)$ represents loudspeaker input signals at discrete time t, while the $M \times 1$ vector $y(t)$ is the sound sampled at the control points.

The noise components to be controlled are described by noise paths (primary paths) from $r(t)$ modeled by an $M \times L$ FIR matrix,

$$z(t) = \boldsymbol{D}(q^{-1})\, r(t) \ . \tag{2}$$

Spectral properties of $r(t)$ are furthermore represented by a stable vector-autoregressive model

$$r(t) = \boldsymbol{H}^{-1}(q^{-1})\, e(t) \ , \tag{3}$$

where the $L \times 1$ vector $e(t)$ is white, with zero mean and covariance $\mathbf{R_e}$.

The LQG feedforward regulator is a linear rational matrix

$$u(t) = -\boldsymbol{\mathcal{R}}(q^{-1})\, r(t+d) \ , \tag{4}$$

of dimension $N \times L$, resulting in a control error vector

$$\varepsilon(t) = z(t) + y(t) = (q^{-d}\boldsymbol{D} - \boldsymbol{B}\,\boldsymbol{\mathcal{R}})r(t+d) \ . \tag{5}$$

The control paths $\boldsymbol{B}\,\boldsymbol{\mathcal{R}}$ are made to approximate the "target" $q^{-d}\boldsymbol{D}$ that represents the noise paths, or primary paths, delayed by d samples. Use of a longer delay results in a higher approximation fidelity. However, to compensate for this the regulator (4) needs to act on a time-shifted (predicted) feedforward signal $r(t+d)$. For narrowband noise $r(t)$, prediction can be performed with high precision while this is not the case for broadband noise. We will use $d \gg 0$ in designs for narrowband noise below, while $d = 0$ is used for broadband designs.

The design aims to minimize the scalar quadratic criterion

$$J \quad = \quad E\{(\boldsymbol{V}\varepsilon(t))'\boldsymbol{V}\varepsilon(t) + (\boldsymbol{W}u(t))'\boldsymbol{W}u(t)\} \ , \tag{6}$$

under constraints of stability and causality of $\boldsymbol{\mathcal{R}}(q^{-1})$. The weighting $\boldsymbol{V}(q^{-1})$ is an $M \times M$ polynomial matrix of full normal rank M. The square polynomial matrix $\boldsymbol{W}(q^{-1})$ can be used to focus the control energy to appropriate frequencies, and into spatial subspaces that are appropriate for the room and the sound system. For example, when $\boldsymbol{W}(q^{-1}) = \mathrm{diag}[W_j(q^{-1})]$, each scalar penalty FIR filter $W_j(q^{-1})$ can be given low gain within the operating range of loudspeaker j and high gain outside of that range.

The problem becomes a special case of a MIMO LQG feedforward regulator design problem in input-output form discussed in [9]. The solution is obtained by first computing an $N \times N$ polynomial matrix $\boldsymbol{\beta}(q^{-1})$, that has a stable and causal inverse, from the spectral factorization equation

$$\boldsymbol{\beta}_*\boldsymbol{\beta} = \boldsymbol{B}_*\boldsymbol{V}_*\boldsymbol{V}\boldsymbol{B} + \boldsymbol{W}_*\boldsymbol{W} \ . \tag{7}$$

Such a matrix is guaranteed to exist under mild conditions, for example by the use of a penalty matrix $\boldsymbol{W}$ such that $\det[\boldsymbol{W}(z^{-1})] \neq 0$ on the unit circle.

A causal $N \times L$ polynomial matrix $\boldsymbol{Q}(q^{-1})$ is then, together with an $N \times L$ polynomial matrix $\boldsymbol{L}_*(q)$, obtained as the unique solution to the polynomial matrix Diophantine equation

$$q^{-d}\boldsymbol{B}_*\boldsymbol{V}_*\boldsymbol{V}\boldsymbol{D} = \boldsymbol{\beta}_*\boldsymbol{Q} + q\,\boldsymbol{L}_*\boldsymbol{H} \ . \tag{8}$$

The unique stable linear regulator (4) that minimizes the criterion (6) for the model (1), (2), (3) is then the IIR filter

$$u(t) = -\boldsymbol{\beta^{-1}}(q^{-1})\,\boldsymbol{Q}(q^{-1})\, r(t+d) \ . \tag{9}$$

See Section 3.3 of [9] for a proof. We truncate the pulse responses and realize the controller with FIR filters.

3. EXPERIMENTAL EVALUATION

3.1. Method and Assumptions

All experiments were performed in a room with dimensions $4.6 \times 6 \times 2.6$ m. Microphones were placed uniformly in a grid with 4×4 control points covering 0.3×0.3 m. The grid was placed above a sofa at a height corresponding to the ears of a person sitting in the sofa. Eight ATC SCM16 speakers were placed around the sofa as illustrated in Fig. 1. One of these speakers, placed 1.45 m behind the sofa, was used as the noise source and will be referred to as the noise speaker below. The seven other speakers were used as control

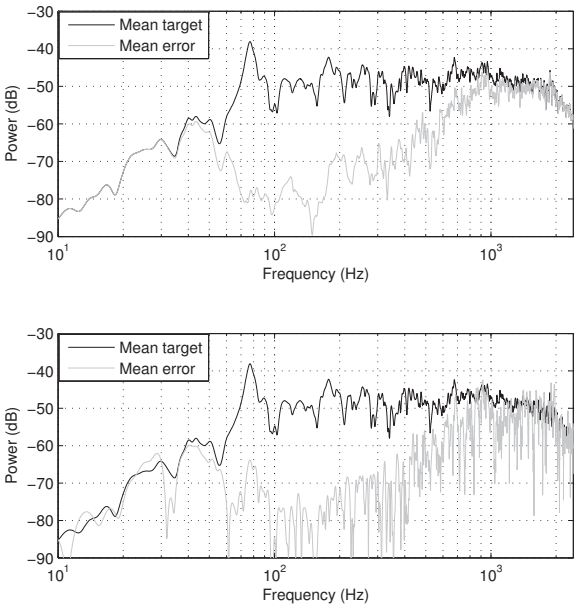

Fig. 4: MIMO narrowband design ($d = 0.1$ s) noise suppression potential. Top) Simulation results for the narrowband design. Bottom) Results after validation measurements. The black curve is the RMS average of the target spectra $|\boldsymbol{D}(e^{-j2\pi f})|^2$ at the 16 microphone positions, and the gray curve is the RMS average of the control errors.

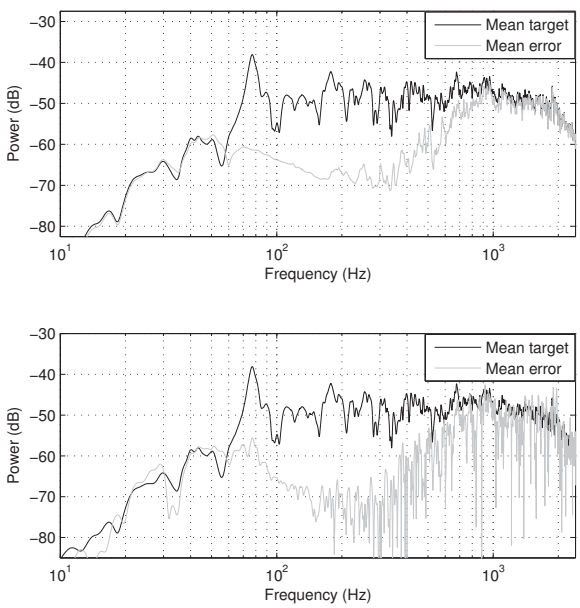

Fig. 5: MIMO broadband design ($d = 0$) noise suppression potential. Top) Simulation results for the broadband design. Bottom) Results after validation measurements. The black curve is the RMS average of the target spectra $|\boldsymbol{D}(e^{-j2\pi f})|^2$ at the 16 microphone positions, and the gray curve is the RMS average of the control errors.

speakers. The input to the noise speaker was used as feedforward signal ($L = 1$). It should be noted here that this assumption of full knowledge of the noise source is unrealistic in a practical implementation. However, we use it in this work to show the full potential of the method. Generation and prediction of the feedforward signal is regarded as a separate problem.

FIR models of order 19999, sampled at 48 kHz of the impulse responses from each loudspeaker to each microphone position were estimated. Sine sweeps were used as excitation signals (see [12]), with 9 sweep periods for each impulse response. The power spectral density (PSD) of the estimated impulse responses from the noise speaker is shown in Fig. 3 for frequencies up to 2400 Hz.

Using the estimated impulse responses, subsampled to 4.8 kHz, narrowband and broadband regulators were designed. The modeling delay was set to $d = 0.1$ s for the narrowband case and to $d = 0$ s for the broadband case. In both cases, the weighting matrix $\boldsymbol{W}(q^{-1})$ in (7) was set to be diagonal, with the diagonal elements having a magnitude of -30 dB in the frequency range $60 - 1500$ Hz and a high gain outside of it, for all loudspeakers. The weighting matrix $\boldsymbol{V}(q^{-1})$, as well as $\boldsymbol{H}(q^{-1})$, were set to unit matrices.

For comparison, SISO regulators were constructed using one loudspeaker and one microphone position, both marked in Fig. 1. The same modeling delays as in the MIMO case were used in the SISO designs. However, for the SISO narrowband case, the possibility of incorporating the noise characteristics into the design equations via the AR model in (3) was fully taken advantage of. This leads to one design per narrowband test signal. The SISO control speaker was chosen to be the one with the most similar spatial properties as the noise speaker (see Fig. 1). The weighting $\boldsymbol{W}(q^{-1})$ was chosen to be scalar, with value 10^{-5}.

Simulations were performed to evaluate the performance of all the designs. Validation measurements at the control points were conducted both to test the target noise path ($q^{-d}\boldsymbol{D}$) reproduction accuracy through the regulator and to see how well actual noise signals were attenuated. For the later purpose, three different single tone experiments with frequencies 200, 400 and 600 Hz were performed, as well as an evaluation for a broadband noise, with energy content in the frequency range $60 - 700$ Hz. For the purpose of validating the reproduction quality of the target path, the same sine sweeps were used as in the original system identification.

3.2. Results

Fig. 4 shows the results from the narrowband MIMO design. The top part shows the RMS averages, both for the PSD of the target over the 16 microphone positions and for the PSD of the errors between the target impulse responses and the simulated resulting impulses response. The bottom part shows the same curves from the validation measurements. The power of the error, relative to the target, indicates the attainable power of the remaining noise after cancellation. Worth noting is that simulated and measured results are very similar in shape, which is the case for all the results, including those given only for measured data below. A good signal to noise ratio in the identification resulted in accurate system models.

Although Fig. 4 shows the accuracy in the frequency domain of the results, it fails to incorporate the effect of the modeling delay in the time domain. Choosing a modeling delay larger than 0 causes the impulse responses of the control path to have pre-ringings. These pre-ringings are mainly affecting the higher end of the spectra.

The levels of attenuation achieved for the three sinusoid signals are shown in Table 1 for the MIMO design and in Table 2 for the SISO designs. Here we note that the MIMO design can achieve a silent zone throughout the area of interest whereas the SISO designs, as expected, fail to do so. It is interesting to see that for the MIMO

Table 1: Attenuation at the 16 microphone positions for the MIMO narrowband design at 200, 400 and 600 Hz.

200 Hz			
29.9 dB	23.0 dB	23.9 dB	28.6 dB
18.2 dB	25.7 dB	24.3 dB	16.8 dB
19.4 dB	25.9 dB	23.6 dB	16.5 dB
35.1 dB	25.1 dB	29.1 dB	25.0 dB
400 Hz			
19.7 dB	22.5 dB	24.9 dB	19.5 dB
26.0 dB	21.9 dB	19.7 dB	24.3 dB
24.3 dB	18.5 dB	14.8 dB	13.3 dB
14.6 dB	12.9 dB	13.7 dB	11.8 dB
600 Hz			
4.3 dB	4.6 dB	7.0 dB	20.0 dB
9.8 dB	9.2 dB	5.6 dB	2.6 dB
15.3 dB	7.9 dB	7.8 dB	10.1 dB
5.1 dB	7.4 dB	8.2 dB	6.6 dB

Table 2: Attenuation at the 16 microphone positions (target position for the regulator design in bold) for SISO narrowband design.

200 Hz			
7.5 dB	9.3 dB	8.0 dB	5.4 dB
9.8 dB	14.7 dB	13.3 dB	8.6 dB
12.4 dB	22.1 dB	16.6 dB	9.6 dB
15.3 dB	**31.6 dB**	15.0 dB	8.5 dB
400 Hz			
0.5 dB	3.5 dB	5.1 dB	1.7 dB
1.1 dB	3.2 dB	4.9 dB	3.3 dB
2.8 dB	5.0 dB	7.1 dB	5.5 dB
10.8 dB	**28.4 dB**	12.5 dB	16.1 dB
600 Hz			
-1.8 dB	19.2 dB	-2.0 dB	-5.0 dB
-3.1 dB	0.8 dB	0.8 dB	-3.4 dB
-3.5 dB	1.7 dB	1.1 dB	0.5 dB
1.4 dB	**19.4 dB**	1.5 dB	3.2 dB

design, the zone of silence is rather uniform even at 400 Hz. At 600 Hz, however, the attenuation has started to become quite dispersed.

The accuracy and noise reduction potential remains large also for the MIMO broadband design, using $d = 0$, with results shown in Fig. 5. A performance reduction in the broadband design due to the lack of modeling delay can be seen in Fig. 5, particularly in the lower frequency range.

Finally, a broadband signal with the frequency range 60-700 Hz was sent through the MIMO system, with and without control. The spectral content of the result (RMS average) can be seen in Fig. 6. The result is similar to that expected from the mean error results in the sine sweep validation measurements of Fig 5. An attenuation of more than 10 dB was obtained at almost all frequencies in the range $70 - 500$ Hz. Significant attenuation was also attained for $500 - 700$ Hz, a frequency region where transfer functions from individual loudspeakers are extremely irregular and vary between control points, see Fig. 3.

Acknowledgements: The authors gratefully acknowledge the support from the Knut and Alice Wallenberg foundation (Dnr. KAW 2006.0152), which provided funding for acoustic measurement equipment. We thank Lars-Johan Brännmark for comments and for software tools used.

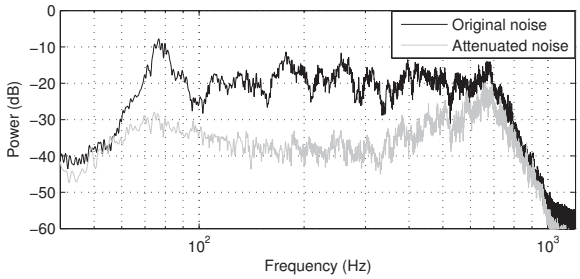

Fig. 6: Results from real time cancellation of a broadband noise signal with energy in the frequency range 60-700 Hz. The black curve is the frequency content of the original noise, and the gray curve is the frequency content after attenuation.

4. REFERENCES

[1] S.M. Kuo and D. R. Morgan, "Active noise control: A tutorial review," *Proc. IEEE*, vol. 87, no. 6, June 1999, pp. 943-973.

[2] H. Sano, T. Inoue, A. Takahashi, K. Terai, and Y. Nakamura, "Active control system for low-frequency road noise combined with an audio system," *IEEE Trans. on Speech and Audio Processing*, vol. 9, no. 7, Oct. 2001, pp. 755-763.

[3] B. D. Radlovic, R.C. Williamson, and R.A. Kennedy, "Equalization in an acoustic reverberant environment: robustness results," *IEEE Trans. on Speech and Audio Processing*, vol. 8, no. 3, pp. 311-319, May 2000.

[4] S. Spors, R. Rabenstein and J. Ahrens, "The theory of wave field synthesis revisited", Presented at *AES 124th Convention, Amsterdam*, preprint 7358, May 2008.

[5] M. A. Poletti, "Three-dimensional surround sound systems based on spherical harmonics," *J. Audio Eng. Soc.*, vol. 53, no. 11, pp. 1104-1025, Nov. 2005.

[6] S. J. Elliott and P. A. Nelson, "Multiple-point equalization in a room using adaptive digital filters," *J. Audio Eng. Soc.*, vol. 37, no. 11, pp. 899–907, November 1989.

[7] S.J. Elliott, I.M. Stothers and P.A. Nelson, "A multiple error LMS algorithm and its application to the active control of sound and vibration", *IEEE Trans. on Acoustics, Speech and Signal Processing*, vol. 35, No. 10, Oct. 1987, pp 1423-1434

[8] Y. Huang, J. Benesty and J. Chen, *Acoustic MIMO Signal Processing*, Springer, New York, 2006.

[9] M. Sternad and A. Ahlén, LQ Controller Design and Self-tuning Control. Chapter 3 in K. Hunt Ed, *Polynomial Methods in Optimal Control and Filtering*, Control Engineering Series, Peter Peregrinus, London, Jan. 1993, pp. 56–92.

[10] M. Johansson, L-J Brännmark, A. Bahne and M. Sternad, "Sound field control using a limited number of loudspeakers," *AES 36th Int. Conf.*, Dearborn, Michigan, US, June 2-4 2009.

[11] L-J Brännmark, *Robust Sound Field Control for Audio Reproduction: A Polynomial Approach to Discrete-Time Acoustic Modeling and Filter Design.* Ph.D Thesis, Dept. of Engineering Sciences, Uppsala University, January 2011.

[12] S. Müller and P. Massarani, "Transfer-function measurement with sweeps," *J. Audio Eng. Soc.*, vol. 49, no. 6, pp. 443–471, June 2001.